Adaptive Welding by Fiber Optic Thermographic Sensing: An Analysis of Thermal and Instrumental Considerations

Fiber optic sensing system which views thermal emission directly from the surface being welded offers more accurate in-process response to welding variables encountered in an adaptive robot operation

BY J.P. BOILLOT, P. CIELO, G. BÉGIN, C. MICHEL, M. LESSARD, P. FAFARD, AND D. VILLEMURE

ABSTRACT. Real-time thermographic inspection during welding is a promising approach for quality monitoring and adaptive process control. We present a numerical analysis of the dynamic thermal distribution and infrared emission from the weld surface showing the correlation between the thermographic features and the welding variables to be controlled in adaptive welding. On the experimental side, we review the work performed at our institute during the last years for the development of a discrete-point thermographic sensing system. As our theoretical analysis shows, discrete-point sensing can be a valid alternative to the more expensive and bulky thermal imaging approach for thermographic welding control. We describe in detail a fiber optic array sensor mounted inside the welding torch which is very compact, fast and rugged.

Introduction

The modern industrial trend towards robotic welding reflects the need for an increased productivity and an improved quality of the welded products (Refs. 1, 2). Manual welding must be limited to short periods because of operator discomfort and safety problems, and manual welding arc time is generally less than 30% of the total operator working time. Moreover, the possibility of an increased welding speed, as well as in-process welding quality control, provides strong motivation to develop advanced robotic welding techniques (Refs. 3, 4).

The quality of robotic welding is now limited by the difficulty to adapt the robot to the welding process variables, which include unwelded parts variables, weld machine variables, metallurgical and welding head positioning variables. Unwelded parts variables such as joint mismatch, heat balance, root opening position and width have strong effects on the welding process. Examples of weld machine variables are random fluctuations in current and voltage, arc fluctuations related to plate topographical factors or arc blow, gas composition and flow rate. Metallurgical variables are mainly related to surface contamination and to the visco-dynamic, thermal and interface properties of the base and filler metal. Welding head positioning variables result largely from an inability to maintain tolerances in parts dimensions, parts position in the fixturing equipment and parts distortions during welding. Most of these variables are treated as stochastic parameters in present day robot welding machines because their value is not known during the welding process.

Sensing systems are required to provide adequate in-process information on the physical state of the weld area for a partially or fully adaptive robot operation. Such sensors would track variations in dynamic weld conditions, providing real-time information which would be immediately fed back to the machine controller. This information would update the process status model in the monitoring unit, which after comparison with the stored data base would produce the appropriate corrective actions.

Optical Sensors

Optical sensing systems are under extensive development for adaptive welding applications. The main advantages of the optical approach are noncontact operation, versatility and the availability of a large amount of information from the spatial as well as the spectral features of the optical output. Optical sensing systems can be classified into active or passive, depending on whether the observed image is produced by selective illumination with an artificial light source such as a laser, or whether the welding scene is observed without artificial illumination. Passive systems can be divided into reflective or emissive systems, depending on whether the observed visual pattern is produced by reflection of the ambient light from the inspected object, or whether the observed light pattern is produced by direct thermal emission from the hot

---

J.P. BOILLOT and D. VILLEMURE are with Servo-Robot, Boucherville, Québec, Canada. P. CIELO is with the Industrial Materials Research Institute, Boucherville, Canada. C. MICHEL and P. FAFARD are with the Welding Institute of Canada, Boucherville, Canada. G. BÉGIN is with the Hydro-Québec Research Institute, Varennes, Canada. M. LESSARD is with Ecole Polytechnique de Montréal, Montreal, Canada.

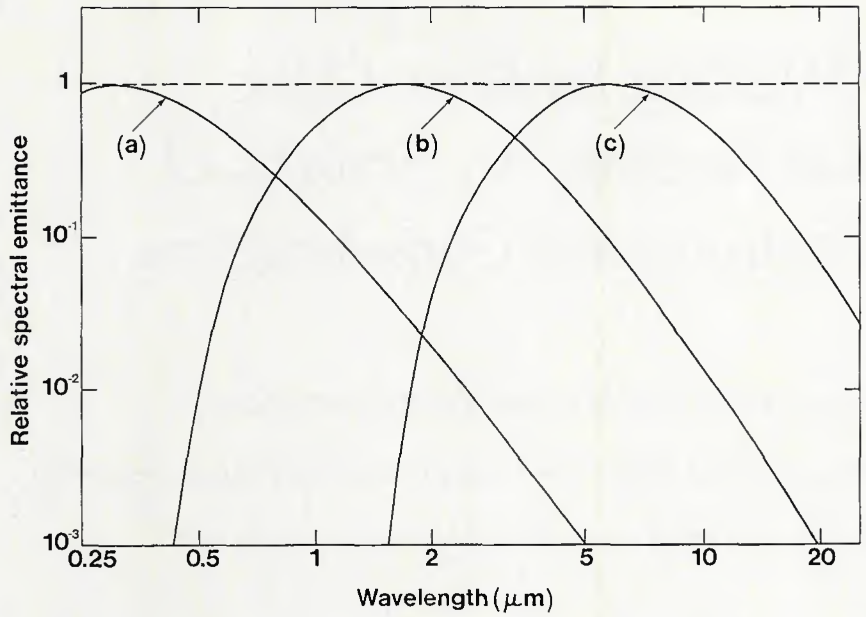

Fig. 1 — Relative blackbody emittance vs. wavelength at a temperature of (A) 10,000 K, (B) 1800 K and (C) 500 K. The absolute emittance scale is different for the three curves

surface. Most of the active sensing systems use pattern projection and triangulation techniques to obtain the surface profile in front of the welding pool for robot arm guiding and arc control purposes (Refs. 5-8). The optical pattern is projected at a certain distance from the weld pool in order to avoid arc reflection and thermal emission background noise. Although such techniques are very powerful, closer operation would be preferred to avoid excessive delay, need for angularly decoupling the inspection system from the welding head, and to account for thermal distortions near the weld pool. Similar considerations can be made concerning inspection systems using a "learn run" (Ref. 9).

Passive optical sensors have recently been used to view directly the thermal emission from the surface being welded (Refs. 10, 11). The possibility to inspect in real-time the temperature of the welded materials is very attractive because the temperature distribution around the weld pool provides important information on the welding status. Factors such as the pool shape, absolute temperature, and symmetry of the temperature distribution are directly related to several welding process variables, such as joint mismatch, root opening and plate thickness fluctuations, arc blow or the visco-dynamic and thermal conductivity properties of the plates. However, optical inspection by a video camera or a photodiode array operating in the 0.4 to 1 μm spectral range is limited to the weld pool and the surface immediately adjacent to the weld pool, because thermal emission in this spectral range falls abruptly at temperatures lower than 1000 K. Moreover, arc shielding problems are important in this spectral range because of the large amount of radiation emitted by the high temperature arc (10,000 to 15,000 K average temperature) in the short wavelength region. Figure 1 shows the relative blackbody emission spectra at 10,000 K, 1800 K (melting temperature of steel) and 500 K. As we can see, operation in the longer wavelength spectral region is preferable in order to increase the signal-over-arc-background ratio. Long wavelength thermographic inspection during welding has recently been proposed for the thermal characterization of the welding process (Refs. 12-15). Strong correlation was found between the temperature distribution around the weld pool and the welding factors such as arc position and presence of contaminants.

In order to analyze the potential of this approach, a numerical study of the thermal distribution around the weld pool and of its relation to the welding variables has been carried out at our institute. The results of this analysis are described in the next section, followed by a review of recent progress at our institute in the

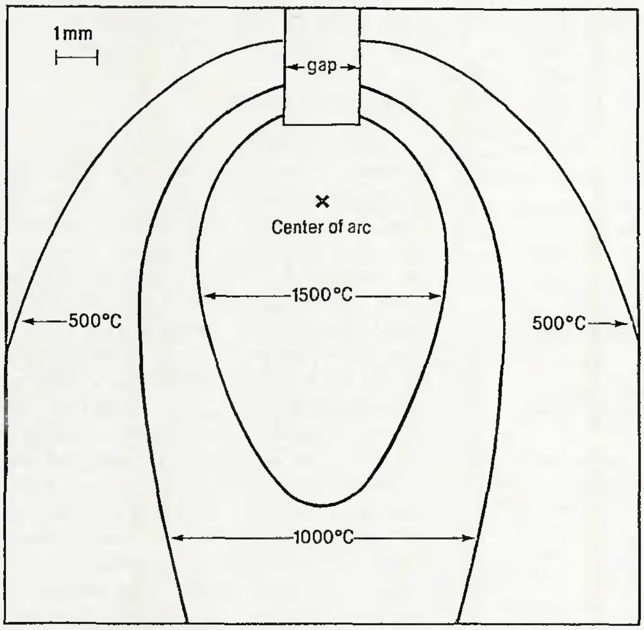

Fig. 2 — Thermal distribution at the surface of the weld area as obtained from the numerical model (carbon steel, weld speed 2.6 mm/s (6.14 ipm))

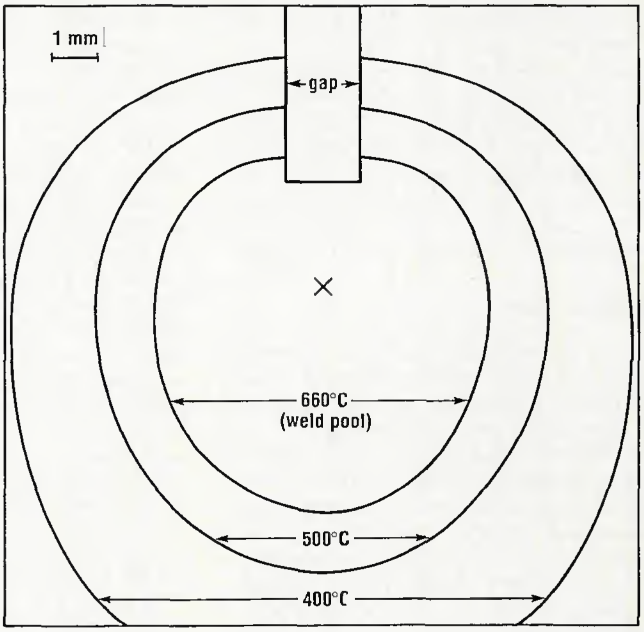

Fig. 3 — Thermal distribution computed for an aluminum plate

development of a fiber optic thermographic sensor and of its application to real-time gas tungsten arc welding process control.

Numerical Analysis

A heat-flow analysis was performed in order to study the effect of various welding settings such as the welding speed, arc position and base metal type on the temperature distribution and thermal emission field at the surface of the plates. The main objective of this study was to provide the required information in the choice of the infrared sensor configuration for optimum control of the welding process.

An analytical solution of the heat flow equation during welding has been given by Rosenthal (Ref. 16) and has been refined by several other authors (Ref. 17). Such analytical models provide a good general idea of the temperature distribution during welding, but they are limited to idealized plate geometries and heat source distributions. Numerical models (Refs. 18, 19) using the finite-difference approach for the solution of the heat flow equation are much more powerful. A numerical model was thus developed at our institute in order to perform the heat flow analysis. The details of our time-resolved model are given in the Appendix.

Figure 2 shows a typical temperature distribution on the surface of the welded area as obtained from such a numerical model. Square-groove carbon steel plates 5 mm (0.20 in.) thick with a 2 mm (0.08 in.) root opening are assumed. The welding arc electric particulars are 17 V, 130 A, with a heat transfer efficiency of 70%. The welding speed is 2.6 mm/s (6.1 ipm). (In Fig. 2, as well as in the following, the welding head movement is assumed to be towards the top of the figure.) In agreement with the previously reported models, the thermal gradient is much steeper in the front of the weld pool rather than in the back. The thermal gradient distribution is strongly related to the thermal diffusivity of the material as well as to the welding speed. Figure 3 shows the thermal distribution when the base metal is aluminum. As expected, the thermal gradient is much smaller and more regularly distributed with aluminum than in the case of Fig. 2, which was obtained for carbon steel. On the other hand, the welding speed strongly affects the thermal gradient in front of the pool, as Fig. 4 shows. This figure shows the position of the 500°C (932°F) isotherm as calculated for carbon steel with welding conditions similar to those of Fig. 2, but for a welding speed of 2 mm/s, 3 mm/s and 3.5 mm/s (4.7 ipm, 7.1 ipm, and 8.3 ipm), respectively. The value of the thermal gradient in front of the pool is an important factor for the choice and position of the infrared sensors, as will be explained later.

Figure 5A shows the effect of arc positioning on the thermal distribution. As we can see, a strongly asymmetrical temperature distribution is obtained on the surface of the plate when the center of the arc is displaced by 1 mm (0.04 in.), with respect to the center of the root opening. Such an asymmetrical pattern is caused by the longer path of the heat flow from the center of the arc to the right plate, as well as by the larger amount of thermal power absorbed by the left plate. It should be noted that the root opening extends partially under the pool, the front of the pool being at 45° with respect to the plate surface, as observed experimentally for this welding configuration. These results suggest the possibility to detect arc displacement by real-time thermographic inspection of the shape and symmetry of the thermal distribution around the weld pool. This is in agreement with recent experimental observations (Ref. 15). Our investigations (Ref. 13) showed that this is a promising approach when combined with a thermographic morphological inspection, as described below.

A question of considerable importance in the choice of a sensor to be used in a feedback configuration is the response time of the feedback loop. In our case, such a response time is mainly limited by the thermal propagation time in the base metal, *i.e.*, the time required for the buildup of the asymmetry in the thermal distribution after the arc was misaligned. Our time-resolved numerical model enabled us to carry out a complete dynamic analysis of the effect of thermal transients, such as an abrupt welding head misalignment or a random-frequency arc fluctuation.

Figure 5B shows the computed thermal response curves at two different positions on the plate surface after the arc is moved 1 mm (0.04 in.) off center, for carbon steel. Curve 1 shows the temperature differential buildup on the front right side of the pool (more precisely, at 5

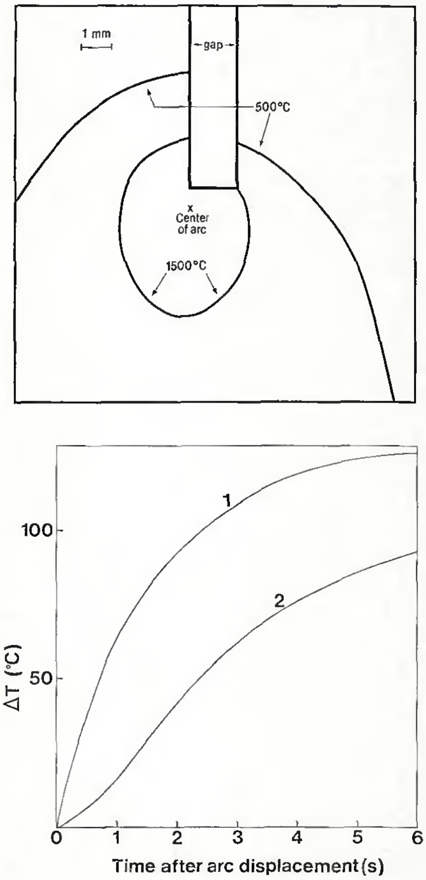

Fig. 5 — (Top) — Thermal distribution in the case of an out of center arc position (carbon steel, 2.6 mm/s). (Bottom) — Thermal response curves after the displacement of the arc for a point at 5 mm (0.20 in.) (curve 1) and at 8 mm (0.31 in.) (curve 2) from the arc

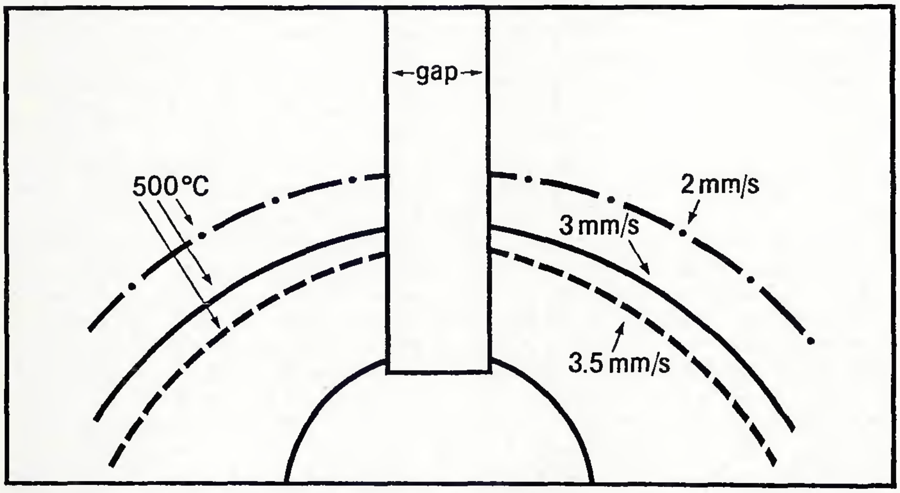

Fig. 4 — Different thermal profiles obtained in front of the weld pool as a function of the welding speed

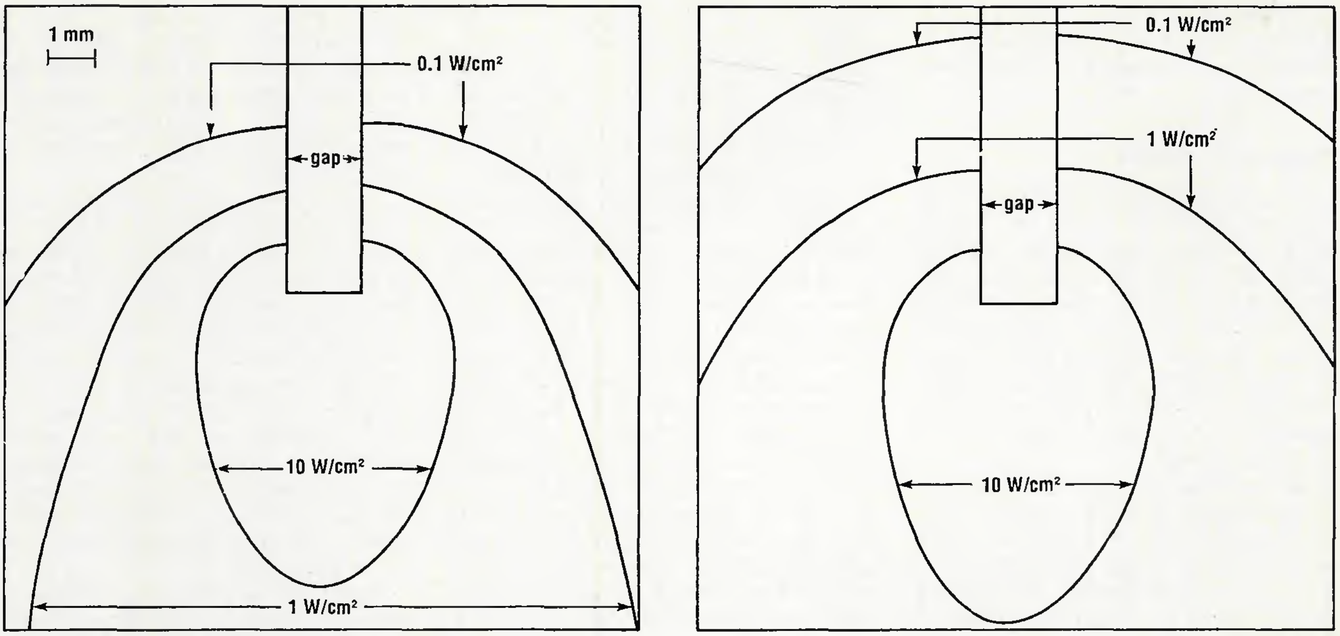

Fig. 6 — Infrared emission from the welded surface integrated over the spectral responsivity of the infrared detector, in the case of (left) a Pbs detector, and (right) an InSb detector

mm (0.20 in.)) from the arc center along a direction making a 45° angle with the joint), while curve 2 is a similar computation for a point situated at 8 mm (0.31 in.) on the right side. Faster response times can be obtained for sampling points situated nearer to the weld pool border, but at the expense of a higher noise produced by pool border fluctuations during welding, as was observed experimentally. Curve 1 shows that a typical response time for the buildup of a detectable asymmetry is approximately one second. Such a delay in the feedback reaction seems to be acceptable when compared to the thermal cycle duration of some seconds in the molten pool.

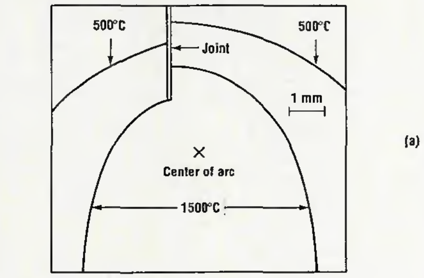

Fig. 7 — (A) Thermal distribution for a narrow gap and misaligned arc; (B) IR radiation along a line situated at 1 mm (0.04 in.) in front of the weld pool

Temperature monitoring in front of the weld pool by infrared sensors is very convenient because it does not require contact with the high temperature surface. However, the infrared emission field from the weld surface may be significantly different from the corresponding temperature distribution, depending on the spectral response of the infrared detector. Figure 6 shows the infrared emission from the surface of the welded area, for welding conditions similar to those leading to the thermal distribution of Fig. 2. The thermal emission signal was integrated over the spectral sensitivity S of the detector, using equation A-8 of the Appendix. For simplicity, the emissivity was assumed constant, which is a satisfactory approximation for the unmelted surface around the pool. No effort was made to account for the emissivity variations inside the weld pool, where the emissivity is typically 2 to 5 times smaller than on the unmelted oxidized surface and where strong fluctuations are produced by the passage of impurities floating on the pool surface (Refs. 12, 13). Figure 6A was obtained by using the spectral responsivity of a PbS detector, which has a detecting bandwidth from 2 to 2.5μm, while Fig. 6B was obtained with an InSb detector, which has a lower sensitivity but a bandwidth from 1 to 5.5μm. As we can see, the infrared emission signal drops steeply in front of the weld pool, decreasing by two orders of value at 3 mm (0.12 in.) in front of the pool in Fig. 6A, and at 5 mm (0.20 in.) in front of the pool in Fig. 6B. Because of detector dynamic range and S/N ratio considerations, it is necessary to monitor the temperature of the surface at a very short distance in front of the pool. This requires a skilled opto-mechanical design to avoid the arc background emission, as well as careful signal processing because of the random fluctuations of the pool borders during welding. Figure 6 shows that a longer wavelength detector such as an InSb is preferable to allow operation at a safer distance from the pool. However, because of the limited spectral transmissivity of the optical fibers used in the inspection system, which will be described in the next section, we are using PbS detectors in our present fiber-optic thermographic inspection system. Optical fibers with longer wavelength responsivity should be available in the near future (Ref. 22), allowing long wavelength operation with an improvement of the system reliability.

Finally, it should be noted that thermal distribution monitoring should be possible also in the case of square groove welding preparations with the plates in close contact, where monitoring by active optical inspection is particularly difficult. Figure 7 shows the computed thermal distribution for a root opening of almost zero thickness when the arc is off center by 1 mm (0.04 in.) with respect to the joint. As the thermal resistivity of the root opening is almost infinite even for very small openings, a finite temperature differential develops across the joint root, as Fig. 7 shows. Such a differential is even

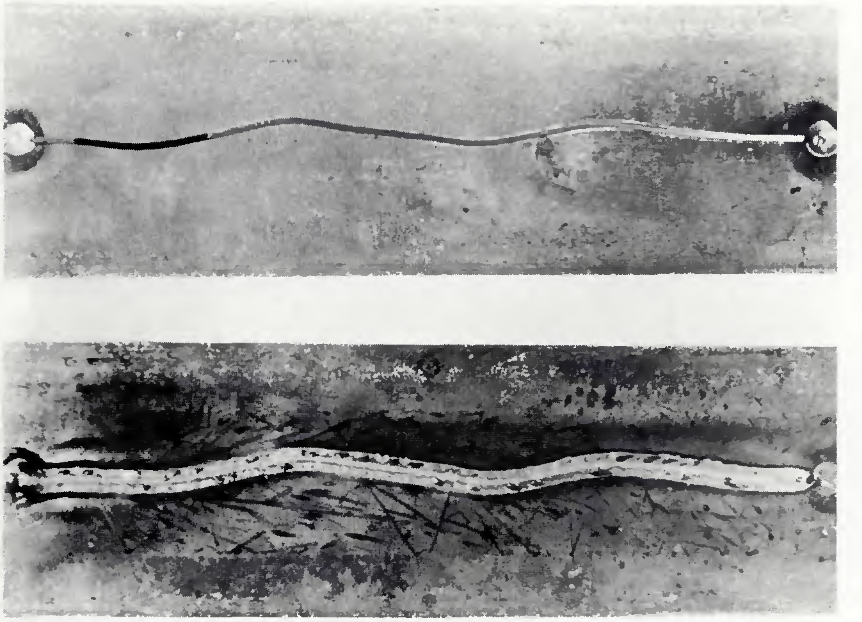

Fig. 8 – Example of an irregular welding path followed by a GMAW head guided by a mechanically scanned fiber optic thermographic sensor, before (top) and after (bottom) welding

more apparent in the infrared emission signal shown in Fig. 7B. This signal would be obtained by scanning with a PbS detector along a line normal to the joint at 1 mm (0.04 in.) in front of the pool. Similar encouraging results were obtained applying our model to lap joint and V-groove welding configurations.

Fiber Optic Thermographic Monitoring System

The numerical model analysis described above shows that most of the required input for robot guiding can be obtained from a relatively small amount of information, such as the temperature distribution along a line in front of the welding pool. This is an interesting consideration because it allows thermographic monitoring by discrete-point thermal inspection, avoiding long and expensive image processing as well as the requirement for bulky and fragile infrared cameras near the welding area. Discrete-point fiber optic monitoring of surface temperature is an attractive opportunity, because only the fiber head must be placed in the hostile environment near the welding head, while the infrared detection and signal conditioning modules can be placed at a safe distance from the welding area. Fiber optic cables have the added advantages of being lightweight and immune from EM interference generated by the arc fluctuations. Fiber optic temperature monitoring in such prohibitive environments as inside a melting furnace has been achieved (Refs. 23-25).

In the last few years, a joint WIC-IMRI-IREQ effort was set up under NRCC funding for the development of suitable sensors for adaptive welding. Both active and passive optical sensors have been developed, and different thermographic sensing configurations were investigated. Preliminary experiments (Ref. 12) were performed with a single spot thermographic sensor pointed on the surface of the base metal at a fixed distance from the weld pool border. Temperature sensing at a fixed point provided information on the width of the pool, and thus indirectly on the depth of penetration. Experiments showed that the highest and fastest temperature variation signals were obtained when the sensor was pointed on the high thermal gradient region in front of the pool, in agreement with the theoretical results discussed previously. Temperature monitoring across the welding pool was also possible with this sensor. Encouraged by these results, a mechanically scanned fiber optic sensor was developed to scan the temperature of the surface in front of the pool for guiding purposes (Ref. 13). A first algorithm simply compared the average temperature on the two sides of the root opening in order to determine the apparent asymmetry of the thermal distribution in front of the pool. This information was sometimes sufficient to guide the welding head, but more reliable results were obtained by combining thermal and morphological information through an IR-vision algorithm, which used both the value and the position of the temperature peaks detected on the borders of the root opening (Ref. 13). Figure 8 shows an example of a curved path joint welded with such a sensor.

In order to increase the scanning speed and to avoid the complexity and bulkiness of mechanical scanning, we recently developed a fiber-array sensor. A schematic view of the sensor is shown in Fig. 9. A fiber optic bundle, typically 5 m (16.4 ft) long, is used to transmit the infrared radiation from the surface in front of the pool to the signal detection and processing unit. The sensor head comprises a lens which forms an image of the fiber ends on the surface. The fiber ends form a linear-array, so that each fiber samples the infrared emission from a point situated along a line on the welded surface, as shown in Fig. 9. This is a convenient method for scanning a line, as opposed to the use of bulky and fragile rotating mirrors or mechanical scanning devices. Another advantage of using a fiber-array to scan a line is the possibility to detect in parallel the signal transmitted by each fiber, with a consequent increase of the S/N ratio as well as of the speed of detection. In the experiments reported here, we used a matrix of 8 PbS detectors to monitor the signal from the 8 fiber array. With a time response of 20 ms for each detector, we could obtain a line sampling rate of 50 lines per second, as compared to 6 lines per second if a single detector with mechanical scanning was used.

As shown in Fig. 1, infrared detection at wavelengths larger than $2 \mu m$ is advisable in order to minimize the arc emission noise. However, commercial silica fibers have a prohibitively high absorptance at wavelengths larger than $2.5 \mu m$, as Fig. 10 shows. We thus decided to use Ge-shielded PbS devices as the infrared detectors, which have a sensitive spectral range from 2 to $2.5 \mu m$. For an emitting surface of 500°C (932°F), which is a typical value of the temperature in front of the weld pool, we are thus operating in the short wavelength end of the infrared emission curve. The spectral emission curve of a black body at 500°C (932°F) is shown in Fig. 10 for comparison. Operation in the short wavelength end of the emission spectrum is convenient because it minimizes the noise produced by emissivity variations of the surface (Ref. 26). However, the absolute value of the detected signal decreases rapidly for lower temperatures, because the peak emission wavelength increases when the temperature decreases. As a result, the minimum detectable temperature was of the order of 300°C (572°F) in our case. As mentioned above, the availability of longer wavelength fibers in the near future should allow operation at lower temperatures if necessary.

Previous experiments were performed with the sensor head fixed in front of the welding head at an angle of observation smaller than 90 degrees to the surface, as Fig. 9 shows. Spurious signals emitted

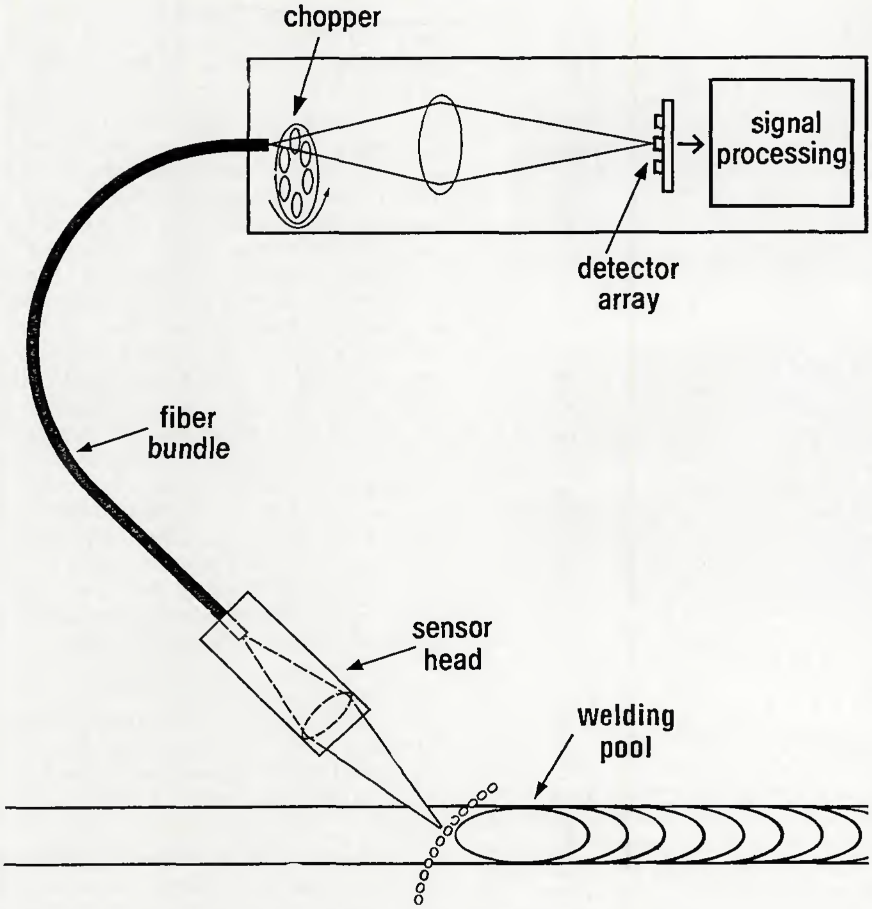

Fig. 9—Schematic view of the linear-array fiber optic thermographic sensor

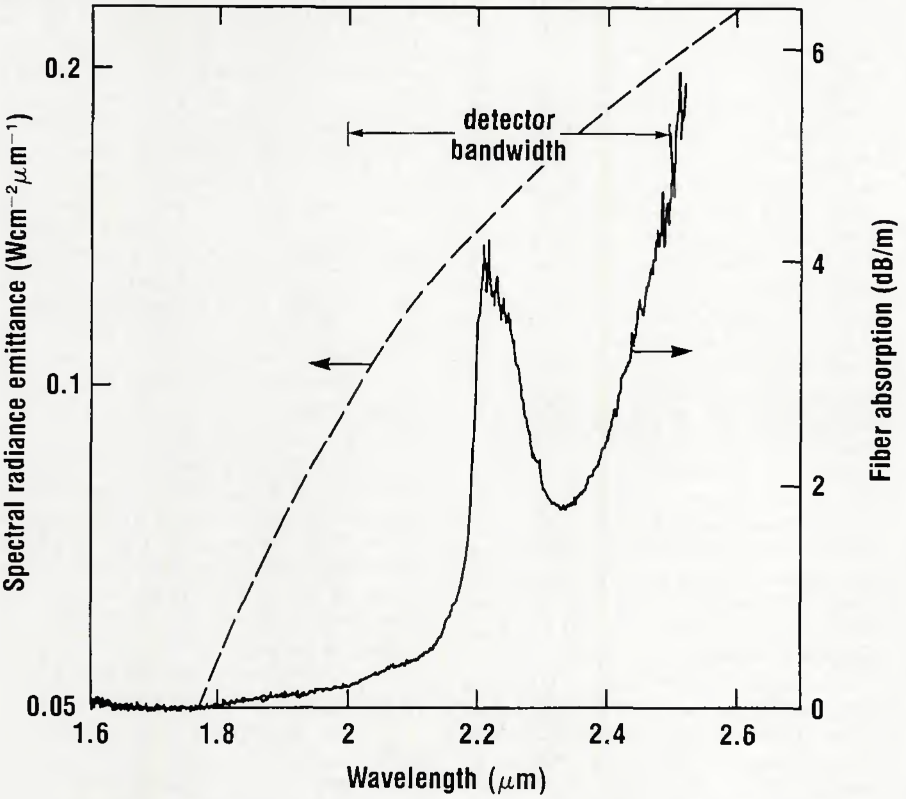

Fig. 10—Measured absorption spectrum of a silica fiber compared with the spectral emission of a surface at 500°C

from the lower portion of the weld pool, as well as arc light reflections, are particularly severe at such a viewing incidence. Moreover, the signal amplitude is strongly dependent on the vertical position of the welding head, because of the strong temperature gradient in front of the weld pool. Using an angle of observation of 90 degrees eliminates those problems, but requires that the sensor head be mounted inside the welding torch, as Fig. 11 shows.

As shown in Fig. 11, the optical sensor was introduced within a GTAW torch. The linear-array fiber bundle was imaged on the surface by an f/4, 15 mm focal length lens. The fiber bundle was a linear array of 8 QSF fibers with core diameter of 200μm and cladding diameter of 280μm. The fiber array was produced by mechanically aligning the fibers, bonding with high-temperature epoxy, cutting and polishing the fiber ends. An optical magnification factor of 2 to 3 resulted in a surface resolution of less than 1 mm (0.04 in.) and a depth of field in the order of 5 mm (0.20 in.). The magnification factor, as well as the sampling position relative to the arc, could be varied by manually adjusting the position of the fiber array by externally placed micrometer screws, while the position of the lens was fixed. Visual tracking of the sampled line on the surface was possible by illuminating two additional fibers which were positioned on each side of the 8 fiber array. A glass plate was placed in front of the lens for protection. Such a plate was replaced or cleaned after a number of welding operations. However, very little plate cleaning was necessary during GTA welding, thanks in part to the protective effect of the inert gas flow.

Figure 12 shows our laboratory prototype of the welding torch with the internally mounted fiber optic thermographic sensor head. The micrometer screw-controlled fiber-holding support can be seen mounted on the right of the welding head. Although this prototype was designed without paying particular attention to the total volume of the device, miniaturized versions of the fiber holding and positioning system would obviously be used in a production oriented unit.

Figure 13 shows a typical signal obtained from the 8 fiber array after synchronous detection with the chopping apparatus shown in Fig. 9 and signal processing by a CAMAC-based system. The sampled line was situated nearly 2 mm (0.08 in.) in front of the pool, and the position of the gap is seen clearly as an abrupt decrease of the apparent temperature in the center of this figure. Several system variables, such as the effect of the welding speed, arc current and tension, gap width and gas flow on the thermal field, are now under evaluation using this

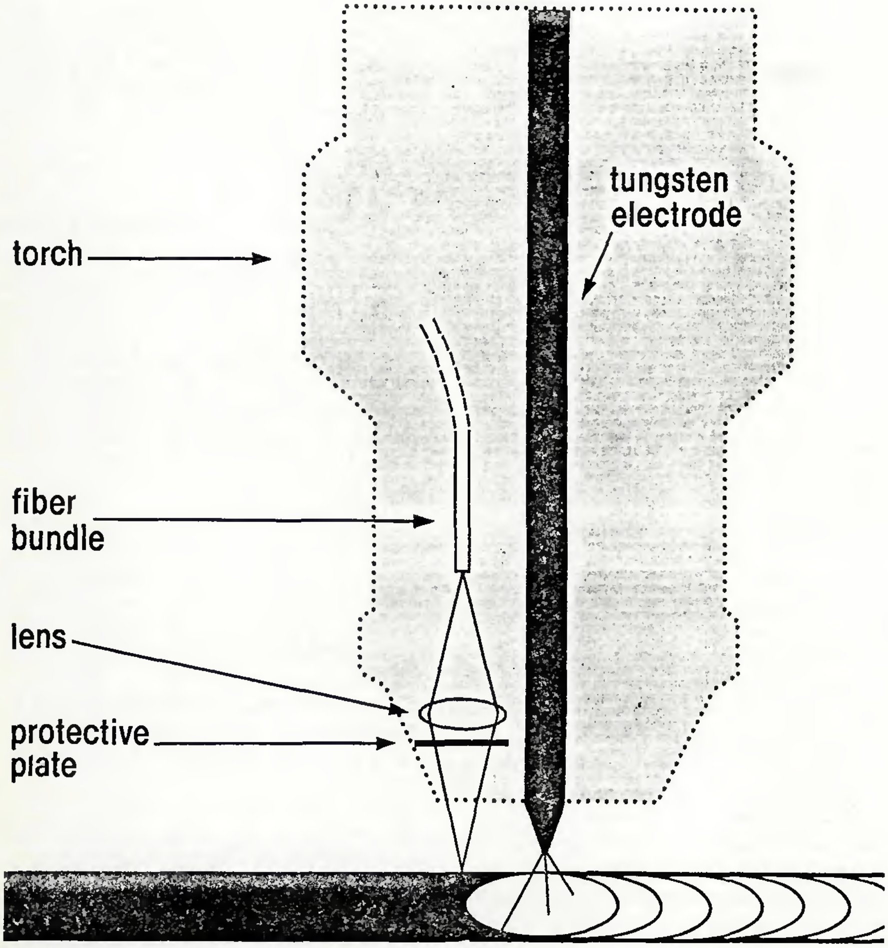

Fig. 11 — Detail of the sensor head mounted inside the welding torch

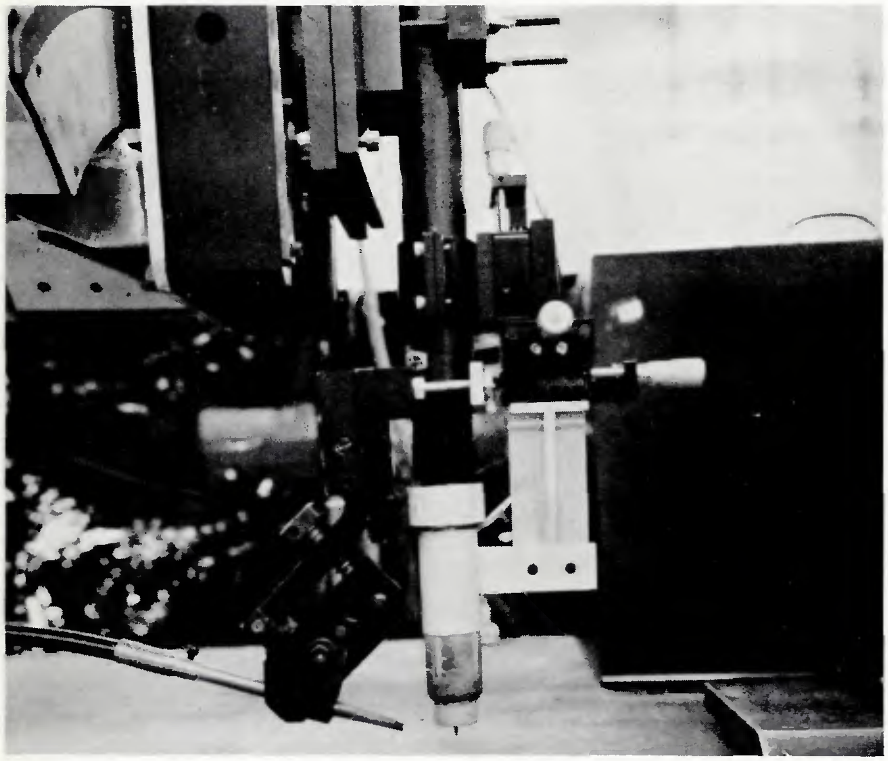

Fig. 12 — GTAW torch with internally mounted fiber optic thermographic sensor head

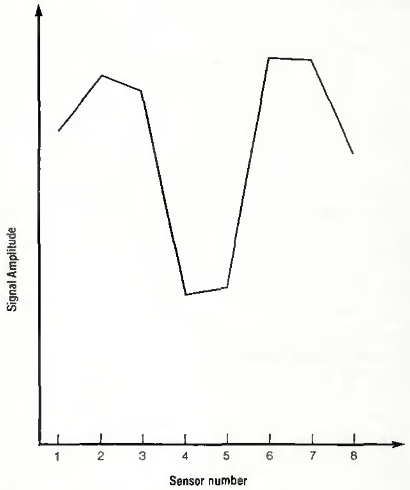

Fig. 13 — Typical signal obtained from the fiber array imaged in front of the welding pool

sensor, and the results will be described in forthcoming technical publications.

Conclusion

Heat flow numerical modelling shows that infrared monitoring provides a powerful tool in adaptive welding. Research work has thus been conducted at the Industrial Materials Research Institute in collaboration with the Quebec Centre of the Welding Institute of Canada for the development of a real-time infrared vision welding system. A miniaturized and rugged fiber optic device coupled to an infrared opto-electronic module under the real-time control of a microcomputer has been completely realized in our laboratory. This approach has been preferred to the use of a conventional infrared camera because of cost, dimensions and ruggedness considerations. This system, presently operational on a welding bench, will be coupled shortly on a welding robot and is expected to bring elements of artificial intelligence which are presently lacking in most flexible automatic welding systems.

Appendix

We describe here the numerical model used for the determination of the temperature distribution as well as of the thermal radiation field reported above.

The three-dimensional finite-difference model used in our computations used the explicit iterative approach to solve the thermal diffusion equation:

$$\frac{\delta T}{\delta t} = \delta\left[\frac{\delta^2 T}{\delta x^2} + \frac{\delta^2 T}{\delta y^2} + \frac{\delta^2 T}{\delta z^2}\right] \qquad \text{(A-1)}$$

by subsequently applying the Fourier equation:

$$\underline{Q} = k_s \text{ grad } T \qquad \text{(A-2)}$$

Table 1

Factors	Value
Temperature of fusion (°C)	1500
Thermal conductivity (watt/cm°C)	From 0 to 900°C: $0.6 - 2.8 \cdot 10^{-4}T$ above 900°C: $0.24 + 1.2 \cdot 10^{-4}T$
Specific heat (joule/g°C)	$0.4 + 2 \cdot 10^{-4}T$
Mass density (g/cm^3)	7.8
Heat of α-γ allotropic transformation (joule/g)	23
Heat of fusion (joule/g)	270
Heat loss by vaporization	$10^4 \exp(6.7 \cdot 10^{-3}T)$
Heat loss by radiation(a) (watt/cm^2)	$2.8 \cdot 10^{-12} (T^4 - 293^4)$
Heat loss by convection(a) (watt/cm^2)	$5 \cdot 10^{-4} (T - 293)$

(a)In these expressions the temperature T is expressed in degrees Kelvin.

and the energy conservation equation:

$$\rho_s C_p \frac{\delta T}{\delta t} = -\operatorname{div} \underline{Q} \tag{A-3}$$

where $\delta = k_s/\rho_s C_p$, is the thermal diffusivity of the base metal, k_s is the thermal conductivity, ρ_s is the mass density, C_p is the specific heat at constant pressure, and $\underline{Q}$ is the thermal flux. This two step approach simplifies the boundary conditions while being more exact when the material properties are temperature dependent and thus spatially nonuniform (Ref. 20).

The model covers a 20 mm × 20 mm × 8 mm (0.79 in. × 0.79 in. × 0.31 in.) volume of the base metal below the welding torch, with an elementary cell of 1 mm^3. Geometrical symmetries are assumed wherever possible. Various geometrical configurations, such as a different pool front slope or bead convexity, can be modelled by distributing air cells within the modelled volume. The temporal iteration is pursued for typical periods of 10 seconds with time increments dt satisfying the stability condition:

$$\frac{\delta dt}{(dx)^2} < \frac{1}{6} \tag{A-4}$$

The initial temperature distribution is uniformly equal to the ambient temperature of 20°C (68°F) if a study of the first 10 seconds after the beginning of welding is to be made. If only the stationary configuration is of interest, an initial temperature distribution decreasing exponentially from the center to the boundaries of the model is assumed to reach more rapidly the stationary distribution.

The 20 mm × 20 mm (0.79 in. × 0.79 in.) modelled area (view from the top) represents the part of the much wider plates to be welded which are under the torch. In order to provide a smooth thermal transition with the rest of the plates which extend infinitely (from a thermal point of view) in the horizontal plane, continuity conditions of the form:

$$\frac{\delta T}{T\, \delta x} = \text{constant} \tag{A-5}$$

are imposed at the metal bounded borders of the modelled volume, while heat losses by radiation, air convection and partial vaporization are assumed at the air bounded surfaces. The expression for such losses, as well as the values of the thermal variables of a typical material (carbon steel) are given in Table 1. The expression for the vaporization losses is obtained from the published data (Ref. 21), while condensation is simulated by reinjecting 75% of the vaporization loss over a 1 cm^2 (0.16 in.^{2}) surface around the weld pool.

The thermal power from the arc is injected over a 20 mm^2 (0.03 in.^{2}) surface on the center of the pool. Typical heat transfer efficiencies of 70% are assumed for GMA welding, and 55% for GTA welding. The injected heat distribution has a nearly gaussian shape. The travel speed is introduced by a linear transformation of the temperature field after each iteration, while the frame of reference is fixed with respect to the arc. Molten filler metal is assumed to penetrate in front of the weld pool at a rate which is equal to the added filler metal in the front plus the metal buildup on the surelevated weld bead in the back of the pool. A portion of the injected thermal power proportional to the added metal and thus to the welding speed is spent for the fusion of the filler metal. The heat of fusion, as well as the heat of the allotropic 720°C (1328°F) transformation (see Table 1), are taken into account through two internal energy matrices which are updated at each temporal iteration. This approach proved to be more reliable than the inclusion of the corresponding peaks in the specific heat expression when such peaks are very narrow.

A radial convective flow is assumed at the surface of the liquid pool, while a downward flow is assumed at the front of the pool within the root opening. Such flow results from several hydrodynamic forces such as the arc pressure, gravity, magnetic stirring, and the resultant of the surface tension components, which depends on the temperature gradient, surface topography and chemical composition of the surface layer. As such factors are hardly predictable, we used a semiempirical approach by using a simplified version of the Navier-Stokes equation at the weld pool surface:

$$\frac{\delta\sigma}{\delta T}\,\frac{\delta T}{\delta x} = \mu\frac{v}{\ell} \tag{A-6}$$

where σ is the surface tension, μ is the temperature dependent viscosity of the liquid metal, v is the flow velocity, and ℓ is the approximated thickness of the flowing layer. For most metals, d σ /dT is temperature independent, while ℓ is nearly constant over the weld pool surface. The following expression was thus used in our model for the velocity of the surface flow:

$$v = \frac{K}{\mu}\,\frac{\delta T}{\delta x} \tag{A-7}$$

where K is a constant whose value is determined empirically by comparing the sectional shape of the modelled pool with the shape obtained by after-welding metallographic inspection.

Finally, the thermal emission field from the weld surface is obtained by integrating the Planck equation:

$$W = \int_0^\infty \epsilon\, S\, (hc^2/\lambda^5)\, (\exp(hc/kT\,\lambda) - 1)^{-1} d\lambda \tag{A-8}$$

where ϵ is the surface emissivity, S is the wavelength dependent sensitivity of the infrared detector, h is Planck's constant, c the light velocity in vacuum, λ the wavelength, and k is Boltzmann's constant. The spectral distribution of the detector sensitivity S is obtained from the manufacturer's specifications, while its absolute value depends on the aperture and the transfer function of the detector optics.

References

1. Vasilash, G.S. 1980. Robots and arc welding: tapping the potential. *Robotics Today* 2:33-34.
2. Sullivan, M.J. 1980. Application considerations for selecting industrial robots for arc welding. *Welding Journal* 59(4):28-31.
3. Meacham, J. 1981. TIG welding with robots. *Robotics Age* 3(3):28-31.
4. Production Division Edition News. 1981. Martin Marietta Orlando Aerospace. *Robotics* 12 (14).
5. Bamba, T., Maruyama, H., Ohno, E., and Shiga, Y. 1982. Welding sensor uses structured light and two-dimensional photocell. *Sensor Review* 2:29-32.
6. Clocksin, W.F., Davey, P.G., Morgan, C.G., and Vidler, A.R. 1982. Progress in visual feedback for robot arc welding of thin sheet steel. *2nd Int. Conf. on Robot Vision and Sensory Controls*. Stuttgart, Germany, Nov. 2-4, 1982.
7. Porter, G.B., and Mundy, J.L. 1982. Noncontact profile sensing system for visual inspection. *SPIE Robot Vision* 336:67-81.
8. Dufour, M., and Bégin, G. 1983. *3rd Int. Conf. on Robot Vision and Sensory Controls.*

Cambridge, England, Nov. 7-10, 1983.

9. Masaki, I., Gorman, R.R., Jordan, D.C., Lindbom, T.H., Dunne, M.J., and Toda, H. 1980. Welding robot with visual seam tracking: Unika-80A. *Int. Conf. on the Developments on Mechanized, Automatic and Robotic Welding.* London, England, Nov. 18-20, 1980.

10. Rider, G. 1975. Measurement of weld pool size by self scanned photodiode arrays. *Proc. Int. Conf. on Low Light and Thermal Imaging Systems.* IEE, London, England.

11. Shende, V.A. 1982. Linear regression modelling of GTAW for developing a real-time feedback control. *CWR Technical Report* 529501-82-4. Ohio State University, Columbus, Ohio.

12. Alexandrov, N. and Boillot, J.P. 1980. Etude exploratoire expérimentale en vue de développer des capteurs pour asservir la puissance d'arc en soudage. *Report ISC-RC 79.* The Welding Institute of Canada, Sept. 1980.

13. Alexandrov, N., Boillot, J.P., and Villemure, D. 1982. Régulation en temps réel du soudage automatique à l'arc électrique. *Report ISC-RC* 88. The Welding Institute of Canada, July 1982.

14. Lukens, W.E., and Morris, R.A. 1982. Infrared temperature sensing of cooling rates for arc welding control. *Welding Journal* 61(1):27-33.

15. Chin, B.A., Goodling, J.S., and Madsen, N.H. 1983. Infrared thermography shows promise for sensors in robotic welding. *Robotics Today* 5:85-87.

16. Rosenthal, D. 1946. The theory of moving sources of heat and its application to metal treatments. Trans. ASME, Nov. 1946.

17. Myers, P.S., Vyehara, O.A., and Borman, G.L. 1967. Fundamentals of heat flow in welding. Welding Research Council Bulletin, No. 123.

18. Paley, Z. and Hibbert, P.D. 1975. Computation of temperatures in actual weld designs. *Welding Journal* 54(11): 385-s to 392-s.

19. Kou, S., Kanevsky, T., and Fyfitch, S. 1982. Welding thin plates of aluminum alloys—a quantitative heat-flow analysis. *Welding Journal* 61(6): 175-s to 181-s.

20. Cielo, P. 1983. Analysis of pulsed thermal inspection. *14th Symposium on NDE.* San Antonio, Texas, April 19-21, 1983.

21. Quigley, M.B.C., Richards, P.H., Swift-Hook, D.T., and Gick, A.E.F. 1973. Heat flow to the workpiece from a TIG welding arc. *J. Phys. D* 6: 2250-2258.

22. Tebo, A.R. 1983. Infrared fibers—promise of the future. *Electro Optics,* June 1983, pp. 41-46.

23. Intrieri, A.J. 1977. Optical fibers look around obstacles to measure temperature. *Control Engineering* 24, Dec. 1977.

24. Kearney, F. 1981. Optoelectronic weld travel speed sensor. US Patent Application No. 268, 219, filed on May 29, 1981.

25. Fihey, J.L., Cielo, P., and Bégin, G. 1983. On-line weld penetration measurement using an infrared sensor. *Int. Conf. on Welding in Energy Related Projects.* Toronto, Canada, Sept. 20-21, 1983.

26. Lawson, W.D. and Sabey, J.W. 1970. Infrared techniques. In *"Research Techniques in NDT,"* R.S. Sharpe, editor. Academic Press, London, p. 447.

WRC Bulletin 299
November 1984

This bulletin contains three reports of work conducted under the guidance of the Subcommittee on Failure Modes in Pressure Vessel Materials of the Pressure Vessel Research Committee of the Welding Research Council. Funding for this three year project was supplied by the American Iron and Steel Institute and the Welding Research Council.

1. "Engineering Aspects of CTOD Fracture Toughness Testing," by G. W. Wellman and S. T. Rolfe. This report presents a study of the crack-tip opening displacement (CTOD) test method as a means of evaluating elastic-plastic fracture. Correlations with Charpy V-Notch, CTOD, J-integral, and stress intensity (K) notch-toughness parameters were investigated.

2. "Three-Dimensional Elastic Plastic Finite-Element Analysis of Three-Point Bend Specimens," by G. W. Wellman, S. T. Rolfe and R. H. Dodds.
   This report summarizes the verification of analytical procedures for use in flawed structures. As a first step toward analyzing the more complex structures of a pressure vessel, the three-point bend specimen was analyzed using both 2-D and 3-D elastic-plastic finite-element analysis methods. CTOD and J values determined from these analyses were compared to the experimental results of the five steels investigated in the first paper.

3. "Failure Prediction of Notched Pressure Vessels Using the CTOD Approach," by G. W. Wellman, S. T. Rolfe and R. H. Dodds.
   This report analyzes the behavior of five notched pressure vessels tested at temperatures such that the failure mode varied from fully ductile to brittle behavior. Both 2-D and 3-D finite-element analyses were used to analytically develop curves of pressure versus opening of the flaw in the vessel. The internal pressures corresponding to the minimum CTOD values obtained from the vessel steels were within 7% of the actual burst pressures.

The results of these works contribute significantly to the understanding and predicting of the different failure modes that can occur in pressure-vessel steels.

The price of WRC Bulletin 299 is $13.50 per copy, plus $5.00 for postage and handling. Orders should be sent with payment to the Welding Research Council, Rm. 1301, 345 E. 47 St., New York, NY 10017.

WRC Bulletin 300
December 1984

Under the direction of the Steering Committee on Piping Systems of the Pressure Vessel Research Committee of the Welding Research Council, the Technical Committee on Piping Systems developed a document on criteria establishment describing their objectives and accomplishments, and three technical position documents that have an effect on the design of piping systems, entitled: 1) Technical Position on Criteria Establishment; 2) Technical Position on Damping Values for Piping Interim Summary; 3) Technical Position on Response Spectra Broadening; and 4) Technical Position on Industry Practice.

The technical Position Documents have been submitted to the ASME Boiler and Pressure Vessel Code Committee and the U. S. Nuclear Regulatory Commission for their use.

The price of WRC Bulletin 300 is $14.00 per copy, plus $5.00 for postage and handling. Orders should be sent with payment to the Welding Research Council, Rm. 1301, 345 E. 47 St., New York, NY 10017.

WRC Bulletin 298
September 1984

Long-Range Plan for Pressure-Vessel Research—Seventh Edition

By the Pressure Vessel Research Committee

Every three years, the PVRC Long-Range Plan is up-dated. The Sixth Edition was widely distributed for review and comment. Up-dated problem areas have been suggested by ASME, API, EPRI and other organizations. Most of the problems in the Sixth Edition have been modified to meet current needs, and a number of new problems have been added to this Seventh Edition.

The list of "PVRC Research Problems" is comprised of 58 research topics, divided into three groups relating to the three divisions of PVRC; i.e., materials, design and fabrication. Each project is outlined briefly in a project description, giving the title, statement of problem and objectives, current status and action proposed.

Because of budget limitations, PVRC will not be able to investigate all of these problems in the foreseeable future. Therefore, the cooperation and efforts of other groups in studying these areas is invited. If work is planned on one of the problems, PVRC should be informed in order to avoid duplication.

Publication of this bulletin was sponsored by the Pressure Vessel Research Committee of the Welding Research Council. The price of WRC Bulletin 298 is $14.00 per copy, plus $5.00 for postage and handling. Orders should be sent with payment to the Welding Research Council, Room 1301, 345 E. 47th St., New York, NY 10017.

WRC Bulletin 296
July 1984

Fitness-for-Service Criteria for Pipeline Girth-Weld Quality

By R. P. Reed, M. B. Kasen, H. I. McHenry, C. M. Fortunko and D. T. Read

In this report, criteria have been developed for applying fitness-for-service analyses to flaws in the girth welds of the Alaska Natural Gas Transmission System pipeline. A critical crack-opening-displacement elastic-plastic fracture mechanics model was developed and experimentally modified. Procedures for constructing curves based on this model are provided. A significantly improved ultrasonic method for detecting and dimensioning significant weld flaws was also developed.

Publication of this report was co-sponsored by the National Bureau of Standards and the Weldability Committee of the Welding Research Council. The price of WRC Bulletin 296 is $16.50 per copy, plus $5.00 for postage and handling. Orders should be sent with payment to the Welding Research Council, Room 1301, 345 E. 47 St., New York, NY 10017.